# NCLX controls hepatic mitochondrial Ca$^{2+}$ extrusion and couples hormone-mediated mitochondrial Ca$^{2+}$ oscillations with gluconeogenesis

Mahmoud Taha[1,6], Essam A. Assali[1,2,3,6,**], Tsipi Ben-Kasus Nissim[1], Grace E. Stutzmann[4], Orian S. Shirihai[2,3,5], Michal Hershfinkel[1], Israel Sekler[1,*]

## ABSTRACT

**Objective:** Hepatic Ca$^{2+}$ signaling has been identified as a crucial key factor in driving gluconeogenesis. The involvement of mitochondria in hormone-induced Ca$^{2+}$ signaling and their contribution to metabolic activity remain, however, poorly understood. Moreover, the molecular mechanism governing the mitochondrial Ca$^{2+}$ efflux signaling remains unresolved. This study investigates the role of the Na$^+$/Ca$^{2+}$ exchanger, NCLX, in modulating hepatic mitochondrial Ca$^{2+}$ efflux, and examines its physiological significance in hormonal hepatic Ca$^{2+}$ signaling, gluconeogenesis, and mitochondrial bioenergetics.

**Methods:** Primary mouse hepatocytes from both an AAV-mediated conditional hepatic-specific and a total mitochondrial Na$^+$/Ca$^{2+}$ exchanger, NCLX, knockout (KO) mouse models were employed for fluorescent monitoring of purinergic and glucagon/vasopressin-dependent mitochondrial and cytosolic hepatic Ca$^{2+}$ responses in cultured hepatocytes. Isolated liver mitochondria and permeabilized primary hepatocytes were used to analyze the ion-dependence of Ca$^{2+}$ efflux. Utilizing the conditional hepatic-specific NCLX KO model, the rate of gluconeogenesis was assessed by first monitoring glucose levels in fasted mice, and subsequently subjecting the mice to a pyruvate tolerance test while monitoring their blood glucose. Additionally, cultured primary hepatocytes from both genotypes were assessed in vitro for glucagon-dependent glucose production and cellular bioenergetics through glucose oxidase assay and Seahorse respirometry, respectively.

**Results:** Analysis of Ca$^{2+}$ responses in isolated liver mitochondria and cultured primary hepatocytes from NCLX KO versus WT mice showed that NCLX serves as the principal mechanism for mitochondrial calcium extrusion in hepatocytes. We then determined the role of NCLX in glucagon and vasopressin-induced Ca$^{2+}$ oscillations. Consistent with previous studies, glucagon and vasopressin triggered Ca$^{2+}$ oscillations in WT hepatocytes, however, the deletion of NCLX resulted in selective elimination of mitochondrial, but not cytosolic, Ca$^{2+}$ oscillations, underscoring NCLX's pivotal role in mitochondrial Ca$^{2+}$ regulation. Subsequent in vivo investigation for hepatic NCLX role in gluconeogenesis revealed that, as opposed to WT mice which maintained normoglycemic blood glucose levels when fasted, conditional hepatic-specific NCLX KO mice exhibited a faster drop in glucose levels, becoming hypoglycemic. Furthermore, KO mice showed deficient conversion of pyruvate to glucose when challenged under fasting conditions. Concurrent in vitro assessments showed impaired glucagon-dependent glucose production and compromised bioenergetics in KO hepatocytes, thereby underscoring NCLX's significant contribution to hepatic glucose metabolism.

**Conclusions:** The study findings demonstrate that NCLX acts as the primary Ca$^{2+}$ efflux mechanism in hepatocytes. NCLX is indispensable for regulating hormone-induced mitochondrial Ca$^{2+}$ oscillations, mitochondrial metabolism, and sustenance of hepatic gluconeogenesis.

[1]Department of Physiology and Cell Biology, Ben Gurion University, Beer-Sheva 8410501, Israel [2]Department of Medicine, Endocrinology, David Geffen School of Medicine, University of California, Los Angeles, CA, 90095, USA [3]Metabolism Theme, David Geffen School of Medicine, University of California, Los Angeles, CA, 90095, USA [4]Center for Neurodegenerative Disease and Therapeutics, Rosalind Franklin University of Medicine and Science. North Chicago, IL 60064, USA [5]Department of Molecular and Medical Pharmacology, University of California, Los Angeles, CA, 90095, USA

[6] Mahmoud Taha and Essam A. Assali contributed equally to this work.

*Corresponding author. E-mail: sekler@bgu.ac.il (I. Sekler).

**Corresponding author. Department of Physiology and Cell Biology, Ben Gurion University, Beer-Sheva 8410501, Israel. E-mail: essam@post.bgu.ac.il (E.A. Assali).

*Abbreviations:* Mitochondrial Na$^+$/ Li$^+$/Ca$^{2+}$ exchanger, (NCLX); mitochondrial Ca$^{2+}$ uniporter, (MCU); inositol triphosphate receptor, (IP$_3$R); Vasopressin, (VP); Norepinephrine, (NE); hepatic glucose production, (HGP); cAMP-responsive element binding protein, (CREB); pyruvate tolerance test, (PTT); pyruvate carboxylase, (PC); thyroid-binding globulin, (TBG); MitoTracker deep red, (MTDR)

Received March 27, 2024 • Revision received June 26, 2024 • Accepted June 27, 2024 • Available online 1 July 2024

https://doi.org/10.1016/j.molmet.2024.101982

## Original Article

## 1. INTRODUCTION

Mitochondrial $Ca^{2+}$ dynamics has a pivotal role in orchestrating cellular bioenergetics, $Ca^{2+}$ signaling, and regulation of cell death [1]. $Ca^{2+}$ enters the mitochondria via the mitochondrial $Ca^{2+}$ uniporter (MCU) complex and is subsequently extruded either through the mitochondrial $Na^+/Ca^{2+}$ exchanger, molecularly termed NCLX, or potentially through a less characterized $H^+/Ca^{2+}$ exchange mechanism remained to be further clarified physiologically and molecularly [2—4].

Calcium signaling has an intriguing metabolic role in the liver [5]. Hepatocytes are distinguished by their abundance of contact sites between the endoplasmic reticulum (ER) and mitochondria, which facilitate localized and efficient transmission of $Ca^{2+}$ signals from the inositol triphosphate receptors (IP$_3$R) to the mitochondrial matrix [6]. Seminal studies showed that hepatic hormones such as glucagon, when applied at physiological concentrations, evoke IP$_3$R-dependent cytoplasmic $Ca^{2+}$ ([$Ca^{2+}$]c) oscillations [5—8]. Hepatocytes demonstrate that each [$Ca^{2+}$]c spike independently propagates from the cytosol to the mitochondria, where it triggers a rise in cellular NADH/ NAD + redox transient ratio [7,9,10] Therefore, hepatic [$Ca^{2+}$] oscillatory waves are intrinsically coupled to metabolism flux and mitochondrial function.

The robust correlation between [$Ca^{2+}$]m oscillations and metabolic alterations in hepatocytes provides a tool for investigating downstream physiological pathways mediated by glucagon activity, especially during the fasting state. Incremental glucagon levels during fasting increase the glucagon-to-insulin ratio in the portal circulation, thereby enhancing the liver glucose output via glycogenolysis and then gluconeogenesis. Regulated allosterically, glycogenolysis facilitates rapid mobilization and depletion of glycogen stores. Gluconeogenesis, however, is a slower, more complex process requiring transcriptional regulation and activation of intertwined pathways that break down essential blocks such as amino acids and fatty acids, thus facilitating sustained and continuous hepatic glucose production. Initially, the role of glucagon in gluconeogenesis was predominantly ascribed to transcriptional mechanisms through the activation of cAMP-responsive element binding protein (CREB), located on the promoters of key gluconeogenic genes such as PEP-CK, pyruvate carboxylase, and others [11]. However, recent studies challenged the dominance of the glucagon-dependent transcriptional pathway in gluconeogenesis induction, and underscored an alternative pathway involving $Ca^{2+}$ signaling through an IP$_3$R isoform, where phosphorylation of INSP$_3$R1 by glucagon-activated PKA was shown to play a prominent role in hepatic glucose production [12,13]. However, it remains unknown whether the canonical mitochondrial $Ca^{2+}$ oscillations contribute to glucagon-dependent gluconeogenesis. Furthermore, the distinct roles of the mitochondrial $Ca^{2+}$ transporters in hepatic $Ca^{2+}$ signaling and in modulating gluconeogenesis remain to be addressed.

A significant challenge in deciphering the role of mitochondrial $Ca^{2+}$ signaling in gluconeogenesis is the unresolved molecular identity for the hepatic $Ca^{2+}$ efflux pathway. Earlier studies, mostly carried out on isolated liver mitochondria, proposed that hepatic mitochondrial $Ca^{2+}$ removal is mediated by a $Na^+$ -independent mechanism, presumably $H^+/Ca^{2+}$-dependent exchange pathway [14]. However, other studies utilizing isolated mitochondria from mice pre-treated with norepinephrine (NE) or other PKA activators demonstrated a significant component of $Na^+$-dependent mitochondrial $Ca^{2+}$ efflux [15—19]. In this study, by employing models of global and conditional hepatic-specific knockout (cKO) for NCLX, we show that NCLX has a critical role in facilitating mitochondrial $Ca^{2+}$ efflux in liver hepatocytes.

Furthermore, our data reveal a dominant $Na^+$-dependent $Ca^{2+}$ extrusion mode in isolated mitochondria as well as permeabilized and intact hepatocytes. Surprisingly, the hepatic ablation of NCLX completely abolished the induction of mitochondrial $Ca^{2+}$ oscillations by hepatic hormones, such as glucagon and vasopressin. Lastly, our findings elucidate a crucial role of NCLX in mediating glucagon-dependent hepatic glucose production during fasting. Remarkably, loss of NCLX inhibited gluconeogenesis, which was tested in hepatocytes and mice, further indicating an indispensable $Ca^{2+}$ signaling and metabolic role for NCLX activity in vitro and in vivo.

## 2. METHODS

### 2.1. Animal models and in vivo procedures

Wildtype C57BL/6NJ mice and NCLX-null (C57BL/6NJ-*Slc8b1*$^{em1(IMPC)J}$/ J) were purchased from Jackson laboratories (Jackson lab, Bar Harbor, ME), and bred in our vivarium. Due to global loss of NCLX from birth in these mice, their use was restricted for in vitro experiments and for validation purposes in a different NCLX-null model. Mice genotyping was performed on earpieces or clipped tails obtained during the weaning of pups. Genotyping was performed following the protocol of Jax laboratories by real-time polymerase chain reaction. The following primers were used to detect NCLX-null$^{-/-}$, Heterozygous$^{+/-}$, or WT$^{+/+}$ mice: Forward primer-GGCTCCTGTCTTCCTCTGTG and Reverse primer-GTGTCCATGGGCTTTTGTG.

In addition, a conditional liver-specific NCLX knockout, NCLX floxed mice containing loxP sites flanking exons 5—7 of the Slc8b1 gene (ch12: 113298759—113359493) was generously provided by Prof. John Elrod [20]. Floxed mice were injected via the tail vein with an AAV8-Cre under the control of a hepatocyte-specific promoter TBG ($1.3 \times 10^{11}$ plaque-forming units per mouse, (107787-AAV8, Addgene, Watertown, MA)). AAV8-TBG-Null (105536-AAV8, Addgene) was injected in floxed littermates of the control group. Animals were used for experiments 5 weeks post-injection.

Experimental procedures conducted on mice were performed in accordance with animal welfare and in compliance with other related ethical regulations. The mice studies were conducted under an approved Institutional Animal Care and Use Committee (IACUC) protocol at Ben-Gurion university. The mice were fed a standard chow diet and maintained under controlled conditions (housing at 22 °C with a 12:12 h light:dark cycle). For selected experiments, mice were fasted with free access to water and were compared with ad libitum mice. For in vivo experiments and analysis, a randomization and a double blinded manner were performed using ear-tagging and random mice numbering systems, which were revealed after the termination of the experiment.

### 2.2. Pyruvate tolerance test

An intra-peritoneal pyruvate tolerance test (IP-PTT) was performed on mice fasted for 8 h. Mice were given a single dose (2 g/kg body weight) of L-pyruvate (Sigma) solubilized in 0.9% saline by IP injection after a baseline glucose check. For glucose measurement, tail veins were punctured, and blood was released and applied onto a glucometer (FreeStyle monitoring system). Circulating glucose levels were then measured at indicated time points after pyruvate injection. Bleeding was stopped by applying pressure with gauze in accordance with IACUC protocol.

### 2.3. Hepatocytes isolation

Hepatocytes were isolated from adult male mice by a two-step collagenase perfusion method, as previously reported [21—23]. In brief, the

liver was perfused through the abdominal inferior vena cava, and the hepatic portal vein was cut through. The organ was washed with Hanks' calcium and magnesium-free buffer for 6 min. After the liver had been freed of blood, the calcium-free buffer was replaced by the liver digest media (17703-034, Thermo Fisher Scientific, Roskilde, Denmark) for 7 min. A perfusion rate of 5 ml/min and a temperature of 37 °C were maintained for both solutions during the entire procedure. After the perfusion, the gallbladder and remnants of the diaphragm were removed, and the liver was rapidly excised from the body cavity and transferred to a sterile Petri dish containing a plating medium. The cells were filtered by a 70-micron strainer. Hepatocytes were then gently washed by low-speed centrifugation at 50 $g$ for 5 min at 4 °C. Cells were then diluted with Percoll (P1644, Sigma–Aldrich) at a ratio of 1:1, centrifuged for 10 min, and the pellet was collected. Hepatocyte viability and yield were determined by trypan blue exclusion, and isolations with only over 70% viability were used. Primary hepatocytes were resuspended and plated in "plating media": (Dulbecco's Modified Eagle Medium (DMEM) (11965092, Thermo) supplemented with 10% Fetal Bovine Serum (FBS) (F2442, Sigma–Aldrich), 100 U/ml penicillin and 100 μg/ml streptomycin (03-031-1B, Biological industries), 2 mM Sodium pyruvate (113-24-6, Sigma–Aldrich), 1 μM dexamethasone (SC-29059, Santa Cruz) and 100 nM insulin (Actrapid, Novo Nordisk)). For imaging experiments, hepatocytes were plated directly on collagen-precoated coverslips at a density of 1 million cells per 20 cm², for seahorse respirometry assays, 8,000 hepatocytes were plated per well, and for biochemical assays, cells were plated at a density of one million cells per well in six-wells plate. Two hours after hepatocytes seeding, media was replaced to remove unattached hepatocytes with a "maintenance medium": (DMEM supplemented with 100 U/ml penicillin and 100 μg/ml streptomycin, 2 mM Sodium pyruvate, 100 nM dexamethasone, 1 nM Insulin and 0.2% Fraction V fatty-acid free bovine serum albumin (BSA, E588, VWR, Radnor, PA)). Cells were kept for 24–36 h.

### 2.4. Cell lines

Clonal HepG2 cells were cultured in low glucose (5 mM) DMEM (MFCD00217342, Sigma–Aldrich, St. Louis, MO) supplemented with 10% FBS, 50 U/ml penicillin, and 5 mM HEPES buffer. For imaging experiments, HepG2 cells were seeded onto collagen-precoated coverslips, and $Ca^{2+}$ imaging was performed 72 h post-seeding.

### 2.5. Fluorometry for liver-isolated mitochondria

Mice livers were perfused with Krebs-Henseleit bicarbonate buffer containing (in mM): 120 NaCl, 4.8 KCl, 1.2 MgSO₄, 1.2 KH₂PO₄, 1.3 CaCl2, 25.3 NaHCO3 and 10 mM-Tris/lactate plus 1 mM-Tris/pyruvate, pH 7.4) supplemented with norepinephrine (1 μM) before isolating the mitochondria as described in Crompton studies [24].

Mitochondria from the livers were then isolated as previously described [25]. Briefly, following the perfusion, livers were removed immediately and sliced into Trehalose isolation buffer (TIB) buffer containing 270 mM sucrose, 10 mM HEPES-KOH (pH = 7.4), 10 mM KCl, 1 mM EDTA, 0.1% BSA, and a freshly supplemented protease inhibitor. The samples were kept on ice throughout the process. The livers were mechanically homogenized using 10 strokes with a Teflon-glass homogenizer, followed by a set of centrifugations to obtain the mitochondria fractions. All the steps were performed in a swinging bucket centrifuge at 4 °C. The homogenate was first centrifuged at 600 $g$ for 10 min to remove nuclei and cell debris. The supernatant was transferred to a new conic tube and centrifuged at 3500 $g$ for 10 min. The resultant pellet was resuspended in TIB buffer and re-centrifuged at 1500 $g$ for 5 min. The supernatant was transferred again to a new conic tube and centrifuged at 5500 $g$ for 10 min. The pellet was then collected, resuspended with TIB buffer, and saved on ice as the mitochondrial fraction. Protein concentration was determined by Bradford assay (500-0006, Bio-Rad, Hercules, California, US).

Extra-mitochondrial $Ca^{2+}$ dye Oregon–Green (Thermo) (0.5 μM) was used to measure mitochondrial calcium uptake and efflux. The dye was added to mitochondria resuspended in a $Ca^{2+}$-free TIB buffer in a cuvette at a protein concentration of 1mg/1 ml. Fluorescence was measured with constant stirring in a cuvette fluorimeter at 496 nm excitation and 524 nm emission, as previously described [26]. Measurements started from baseline, followed by the addition of $Ca^{2+}$ bolus (6 μM) to trigger the mitochondrial calcium influx. Ruthenium red (10 μM) was then added in the presence of $Na^+$ (10 mM) or $NMDG^+$ (10 mM) to monitor the mitochondrial calcium efflux phase rates.

### 2.6. Immunoblotting

Isolated organ tissues were washed in ice-cold PBS, minced, and homogenized in MAS buffer (70 mM sucrose, 220 mM mannitol, 5 mM KH₂PO₄, 5 mM MgCl₂, 1 mM EGTA, 2 mM HEPES pH 7.4). Liver, heart, and lung were mechanically homogenized with 10–15 strokes in Teflon-glass homogenizer until all tissues were solubilized. All homogenates were centrifuged at 1,000 $g$ for 10 min at 4 °C, and supernatants were collected. Protein concentration was determined using Bradford assay (Bio-Rad). Twenty micrograms of protein from tissue homogenates were mixed with 4 × LDS sample buffer and subjected to SDS-PAGE gel electrophoresis. Gels were transferred onto polyvinylidene difluoride membranes using a wet transfer system (Bio-Rad). The membranes were blocked with 5% nonfat dry milk for 1 h and then incubated with the following antibodies: NCLX (1:1000, sc-161921, Santa Cruz), MCU (1:1000, sc-515930, Santa Cruz), VDAC1 (1:500, sc-390996, Santa Cruz) and IP3R1 (1:1000, generously provided by Dr. David Yule at University of Rochester). Antibodies were used according to the manufacturer's instructions. After overnight incubation, membranes were washed with Tris-buffered saline containing 0.1% Tween-20 and then incubated with anti-rabbit IgG secondary antibody coupled to HRP (1:10000, sc-2357, Santa Cruz) for 1 h or an anti-mouse (1:5000, sc-2005, Santa Cruz) solution for 1 h. The membranes were washed again as mentioned above and then exposed to a chemiluminescent protein detection system (Fusion SOLO X, Vilber). Detection was done with the EZ-ECL Chemiluminescence Detection kit for HRP (20-500-120, Sartorius).

### 2.7. Live fluorescence imaging

Kinetic live-cell fluorescent imaging was performed to monitor $Ca^{2+}$ transients using two imaging systems. The first system consisted of an Axiovert 100 inverted microscope (Zeiss, Oberaue, Germany), Polychrome V monochromator (Till Photonics, Planegg, Germany), and a Sensi-Cam cooled charge-coupled device (PCO, Kelheim, Germany). Fluorescence images were acquired with Imaging WorkBench 6.0 software (Axon Instruments, Foster City, CA, USA). The second system consisted of an IX73 inverted microscope (Olympus) equipped with pE-4000 LED light source and Retiga 600 CCD camera. All images were acquired through a × 20/0.5 Zeiss Epiplan Neofluar objective using Olympus cellSens Dimension software.

Cells were pre-loaded with the indicated calcium-specific fluorescent dye at the indicated concentrations for 30 min at 37 °C using a modified Krebs–Ringer's solution containing (in mM): 126 NaCl, 5.4 KCl, 0.8 MgCl₂, 20 HEPES, 1.8 CaCl₂, 15 glucose, 10 lactate, 1 pyruvate, with pH adjusted to 7.4 with NaOH and supplemented with 0.1% BSA. After dye loading, cells were washed three times with fresh dye-free Krebs–Ringer's solution, followed by additional incubation of 30 min to allow for the de-esterification of the residual dye.

For mitochondrial $Ca^{2+}$ measurements $[Ca^{2+}]m$, cells were loaded with 1 μM $Ca^{2+}$-specific dye Rhod2-AM (50024, Biotium, Fremont, CA) that preferentially localizes in mitochondria. Rhod2-AM was excited at 552 nm wavelength light and imaged with a 570 nm-long pass filter as previously described [27].

For cytosolic $Ca^{2+}$ measurements $[Ca^{2+}]c$, cells were loaded either with Fura-2AM ratiometric dye (2 μM) (0102, TEF Labs and F0888, Sigma—Aldrich) or Flou4-AM (2 μM) (1892, Lumiprobe, Cockeysville, MD). Fura-2AM was excited alternately with 340 nm and 380 nm excitations and imaged with a 510 nm long pass filter, as described previously [28,29]. Flou4-AM was excited at 494 nm and imaged at 506 nm.

At the beginning of each experiment, cells were perfused with $Ca^{2+}$-containing Krebs—Ringer's solution supplemented with 0.1% fatty-acid free BSA (E588, VWR). To trigger ionic responses, cells were perfused with supplemented Krebs—Ringer's containing ATP (5 μM) (0220, Amresco), vasopressin (1 nM) (sc-356188, Santa Cruz), or glucagon (100 nM) (16941-32-5, Sigma—Aldrich).

Traces of $Ca^{2+}$ responses were analyzed and plotted using Kaleida-Graph. Oscillatory wave frequencies and the area under the curve (AUC) of each graph were calculated using GraphPad Prism 10. The rate of ion transport was calculated from each graph (summarizing an individual experiment) by a linear fit of the change in the fluorescence ($\Delta F$) for $Ca^{2+}$ influx and efflux over time ($\Delta F/dt$). Rates from $n$ experiments (as mentioned in legends to the figures) were averaged and displayed in bar graphs.

Mitochondrial mass was assessed by staining primary hepatocytes with 200 nM MitoTracker™ Deep Red FM (MTDR) (M22426, Thermo) for 1 h. Cells were washed with PBS 3 times, and a Tecan Spark 10M multimode plate reader was utilized to read fluorescence intensity. MTDR was excited with a 633 nm wavelength, and emission was collected at 665 nm.

### 2.8. Digitonin-permeabilized hepatocytes

To determine the $Na^+$ dependence of mitochondrial $Ca^{2+}$ efflux, a digitonin-permeabilized cell system was assayed as previously described, with modifications detailed below [4]. In brief, isolated hepatocytes were plated on collagen-precoated coverslips, the hepatocytes were washed three times with PBS and loaded with a Rhod2-AM dye (1 μM) and maintained in a sucrose buffer containing (in mM): 220 Sucrose, 10 HEPES, 5 Succinate, 2.5 $KH_2PO_4$, 0.4 EGTA with the pH adjusted to 7.4 with KOH. During incubation time, Cyclosporine A (1 μM) was supplemented to the media. Coverslips were first perfused with 4 μg/ml digitonin-supplemented sucrose buffer (D180-1, Goldbio) for 30 s, and then the coverslips were then washed with digitonin-free buffer. Measurements were started with perfusion of $Ca^{2+}$-free buffer to maintain a baseline, followed by the addition of $Ca^{2+}$ bolus (6 μM). After reaching maximal $Ca^{2+}$ uptake, 10 μM of RR was added to block $Ca^{2+}$ uptake in a solution containing either 10 mM of $Na^+$ or, alternatively $NMDG^+$.

### 2.9. Biochemical assessments

For gluconeogenesis and hepatic glucose production measurements, assays were performed as previously described [30]. In brief, primary mouse hepatocytes were isolated and seeded in six-well plates at a density of $1 \times 10^6$ cells per well and kept in maintenance media. 24 h later, Cells were washed with PBS 3 times and incubated with 1 ml of glucose-free DMEM without phenol red, supplemented with 20 mM sodium lactate and 2 mM sodium pyruvate, 4 mM glutamine, 100 nM dexamethasone and supplemented with fatty-acid free BSA 0.1%. The media contained one of the three treatments: Glucagon (20 nM),

Glucagon and Insulin (20 nM and 100 nM respectively) or a vehicle. After an 8 h incubation, 200 μl of the medium was collected and pelleted at slow centrifugation to remove floating cells or cell debris. 30 μl of supernatant was taken to measure glucose using a colorimetric glucose oxidase assay kit (A22189, Thermo). Glucose values were normalized to the amount of proteins for each individual well. For pyruvate carboxylase activity assessment, an ELISA-based assay was used (K2075, Abcam, Cambridge, MA) according to the manufacturer's instructions.

### 2.10. Respirometry assays

Respirometry assays of primary mouse hepatocytes were performed using the Seahorse Bioscience XFe96 platform (Agilent Technologies, Santa Clara, CA) as previously described [30]. In brief, primary isolated hepatocytes were plated at 8,000 cells/well in a collagen-precoated XFe96 plate. Cells were cultured overnight in plating medium used in the isolation. The next day, growth media was replaced with glucose-free media supplemented with 10:1 mM lactate to pyruvate, and cells were treated with glucagon (20 nM) and or insulin (100 nM) for an 8 h incubation prior to assay. The medium was then replaced with XF DMEM media, pH 7.4, supplemented with glutamine, lactate and sodium pyruvate. Mitochondrial stress tests were performed via sequential injection of 3 μM oligomycin, 3 μM trifluoromethoxy carbonyl-cyanide phenylhydrazone (FCCP), and 2 μM rotenone/anti-mycin A.

Oxygen consumption rates (OCR) were normalized by cell count in each well. Cells were fixed with 4% paraformaldehyde (J61899, Thermo) and stained with 1 μg/ml DAPI (D1306, Thermo). A Tecan Spark 10M multimode plate reader was utilized to read fluorescence intensity at ex/em (358/461).

### 2.11. Quantitative PCR analysis

Total RNA was extracted from liver tissues of conditional NCLX KO mice and their respective controls. Livers were homogenized using Nucle-oSpin RNA Kit lysis buffer (Macherey—Nagel, Germany), and total RNA was purified as described by the manufacturer. 1 μg RNA was converted to cDNA using qScript cDNA synthesis kit (Quanta Biosciences, MA, USA). 20 ng of the cDNA was subjected to realtime PCR procedure (Taqman, Applied Biosystems, Thermo Scientific) using Qpcrbio probe blue Mix Lo-ROX kit as described by the manufacturer (PCR Bio-systems). Primers and probe sequences (Integrated DNA Technologies) are shown in Table S1.

### 2.12. Statistical analysis

GraphPad Prism 10 software was used for statistical analysis, Bio-Render was used to generate schematic illustrations, and Adobe Illustrator was utilized for the graphic design of the manuscript figures. Statistical significance was assessed by two-tailed unpaired Student's $t$-test for two-group comparison, and one-way or two-way analyses of variance (ANOVAs) grouped analyses followed by Tukey's test for multiple-group comparisons. All bar graphs were presented as averaged individual sample values of $n$ measurements $\pm$SEM. A value of $p < 0.05$ was accepted as statistically significant. Symbols of significance used: ns (non-significant), $p > 0.05$, $*p \leq 0.05$, $**p \leq 0.01$, $***p \leq 0.001$.

## 3. RESULTS

### 3.1. NCLX is essential for mitochondrial $Ca^{2+}$ efflux in hepatocytes

To study the role of NCLX in mitochondrial $Ca^{2+}$ efflux in hepatocytes, we first used a conditional hepatocyte-specific NCLX KO (KO) utilizing

the Cre-loxP recombination system for gene targeting [20,31]. Mice with loxP-flanked NCLX alleles (denoted as NCLX$^{fl/fl}$) were tail-vein injected with liver-tropic AAV8 viral vector containing a hepatocyte-specific thyroid-binding globulin (TBG) promoter driving a Cre recombinase expression, or its inactive mutant Cre recombinase that served as control (Figure 1A). To determine if the Cre virus effectively knocked down NCLX, we conducted a western blot analysis, which confirmed ablation of NCLX in the liver tissue, while maintaining the normal differential distribution of NCLX protein levels in other tissues (Figure 1B). Additionally, no alteration in MCU expression was detected in the surveyed tissues (Figure 1C). To study the contribution of NCLX to hepatic mitochondrial Ca$^{2+}$ extrusion, primary hepatocytes from conditional KO (cKO) mice and their respective controls were isolated and stained with the mitochondrial Ca$^{2+}$ reporter Rhod-2 AM. We then induced mitochondrial Ca$^{2+}$ transients by applying ATP-dependent purinergic stimulation, leading to intracellular Ca$^{2+}$ rise and subsequent mitochondrial Ca$^{2+}$ fluxes (Figure 1D). Our results show that in hepatocytes lacking NCLX, mitochondrial Ca$^{2+}$ influx and uptake were unaffected. In contrast, we find a ~2.5-fold slower mitochondrial Ca$^{2+}$ efflux in NCLX cKO compared to control hepatocytes (Figure 1E,F). Additionally, monitoring cytosolic Ca$^{2+}$ transients using a Flou4-AM revealed no alterations in cytosolic Ca$^{2+}$ kinetics or amplitude in primary hepatocytes lacking NCLX (Figure 1G,H).

We extended our examination to an additional mouse model with global deletion of NCLX, using the same experimental settings to monitor mitochondrial and cytosolic Ca$^{2+}$ upon purinergic stimulation. Similarly to the results shown in Figure 1, the mitochondrial Ca$^{2+}$ efflux was compromised in hepatocytes with NCLX deletion, yet Ca$^{2+}$ influx rates were unaffected (Supplementary Figure 1A-C) and

with no alterations in cytosolic Ca$^{2+}$ kinetics (Supplementary Figure 1D,E).

Altogether, the results of this set of experiments indicate that NCLX plays a key role in facilitating hepatic mitochondrial Ca$^{2+}$ extrusion.

### 3.2. NCLX mediates a mitochondrial Na$^+$-dependent Ca$^{2+}$ efflux in hepatocytes

The understanding of the ion-dependence mode essential for mitochondrial Ca$^{2+}$ release in hepatocytes has faced significant challenges, primarily arising from conflicting reports of Na$^+$-dependent versus Na$^+$-independent mechanisms, predominantly from studies done on isolated liver mitochondria [14,32]. To study the monovalent-cation dependence required for hepatic mitochondrial Ca$^{2+}$ extrusion, we employed several approaches. First, we utilized a setup where we loaded primary hepatocytes with Rhod2-AM, then permeabilized the cell membrane by digitonin to facilitate ion permeability, and immediately monitored mitochondrial Ca$^{2+}$. Ionic selectivity required for mitochondrial Ca$^{2+}$ efflux was assessed using either Na$^+$, or NMDG$^+$ as control, or Li$^+$ that is uniquely transported by NCLX [4] (Figure 2A). We initially introduced a Ca$^{2+}$ bolus, which resulted in rapid Ca$^{2+}$ uptake; then, we switched to a Ca$^{2+}$-free solution containing one of the three ions, all of which were applied at the same concentration. Ruthenium Red (RR), which blocks the uniporter, was present in all Ca$^{2+}$-free solutions (Figure 2B). Notably, the presence of extra-mitochondrial Na$^+$ and Li$^+$ activated mitochondrial Ca$^{2+}$ efflux in WT hepatocytes (by ~1.4-fold with Li$^+$ and by ~1.6-fold with Na$^+$ compared to NMDG$^+$). Conversely, NCLX KO hepatocytes did not demonstrate any significant Na$^+$ or Li$^+$-dependent mitochondrial Ca$^{2+}$ efflux when compared to NMDG$^+$ (Figure 2C). Second, we explored the
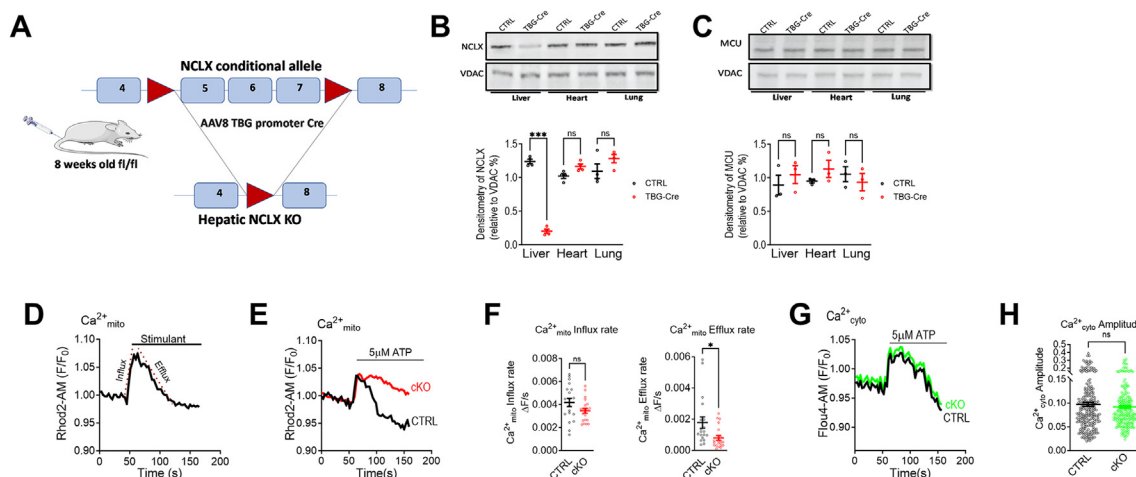


**Figure 1: NCLX is essential for mitochondrial Ca$^{2+}$ efflux in hepatocytes.** (A) Schematic strategy of conditional hepatic NCLX knockout: *(top panel)* Map of *NCLX* gene (slc8b1) with exons 5−7 flanked by two loxP sites. *(bottom panel)* Mice were injected via the tail vein with an AAV8-Cre under the control of a hepatocyte-specific promoter, thyroid-binding globulin (TBG) with subsequent recombination leading to the truncation of the NCLX gene in the hepatocytes only. AAV8-TBG-Null-injected littermates were used as controls. (B) Western blot *(top panel)* and densitometry analysis *(bottom panel)* of NCLX expression in tissues obtained from mice injected either with a hepatic viral Cre vector (TBG-CRE) or TBG-Null (CTRL). VDAC1 was used as a loading control (N = 4 mice per group). (C) Western blot *(top panel)* and densitometry analysis *(bottom panel)* of MCU expression in tissues obtained from mice injected with either hepatic viral Cre vector (TBG-CRE) or TBG-Null (CTRL). VDAC1 was used as loading control (N = 3 mice per group). (D−F) Mitochondrial Ca$^{2+}$ kinetics evoked by ATP in cultured primary hepatocytes isolated from NCLX conditional KO (cKO) mice (cKO, Red) and their controls (CTRL, black). (D) Representative fluorescence transients in primary hepatocytes loaded with the mitochondrial Ca$^{2+}$ dye, Rhod2-AM, application of a stimulus (ATP) at the indicated time and [Ca$^{2+}$]m was monitored. The dashed lines represent the linear fit used to calculate the [Ca$^{2+}$]m influx and efflux rates. (E) Representative [Ca$^{2+}$]m transients of NCLX cKO hepatocytes and their controls (CTRL), triggered by ATP (5 μM). (F) Quantification of [Ca$^{2+}$]m influx and efflux rates for CTRL (n = 19) and cKO (n = 21). (G,H) Cytosolic Ca$^{2+}$ kinetics evoked by ATP in cultured primary hepatocytes isolated from NCLX cKO (cKO, Green) and their controls (CTRL, black). (G) Representative cytosolic Ca$^{2+}$ [Ca$^{2+}$]c transients of cKO hepatocytes, loaded with Flou4-AM, and their controls, triggered by ATP (5 μM). (H) Quantification of [Ca$^{2+}$]c amplitude for CTRL (n = 235) and cKO (n = 244). All values are represented as mean ± SEM, *$p < 0.05$; **$p < 0.01$; ***$p < 0.0001$, N.S- non-significant (two-tailed unpaired $t$-test for comparisons between two groups was used and one-way ANOVA with Tukey's multiple comparison test was used for three or more groups).
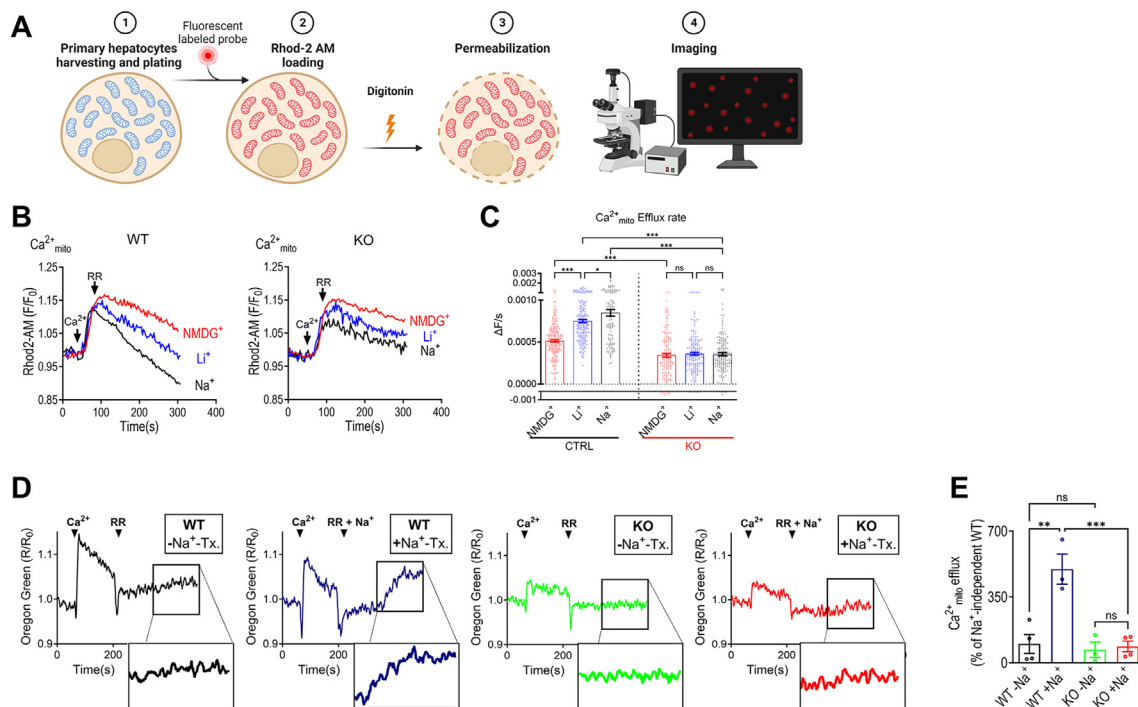
**Figure 2: NCLX mediates Na$^+$-dependent mitochondrial Ca$^{2+}$ efflux in hepatocytes.** (A—C) Analysis of monovalent cation-dependence of [Ca$^{2+}$]m efflux in permeabilized hepatocytes. (A) Schematic cartoon depicting [Ca$^{2+}$]m monitoring in permeabilized primary hepatocytes. (B) Representative traces of [Ca$^{2+}$]m transients in primary WT *(left panel)* and NCLX KO permeabilized hepatocytes *(right panel)*. Ca$^{2+}$ (6 μM) was applied to permeabilized cells and subsequently 10 μM ruthenium red (RR) was applied (at the indicated times). Mitochondrial Ca$^{2+}$ extrusion was monitored in the presence of either 10 mM Na$^+$, Li$^+$ or NMDG$^+$ (used as a cationic replacement of Na$^+$). Detailed experimental design is described in the Methods section. (C) Quantification [Ca$^{2+}$]m efflux rates. WT hepatocytes: (n = 226 for NMDG$^+$, n = 197 for Li$^+$ and n = 109 for Na$^+$); in NCLX-KO hepatocytes: (n = 153 for NMDG$^+$, n = 172 for Li$^+$ and n = 171 for Na$^+$). (D—E) Mitochondrial calcium analysis of isolated mouse liver mitochondria. (D) Representative fluorescent traces of extra-mitochondrial Ca$^{2+}$ transients monitored in isolated mitochondria from liver of WT or NCLX KO mice in the presence of Oregon−Green (500 nM), triggered by the addition of 6 μM free Ca$^{2+}$ followed by the administration of either Na$^+$ or NMDG$^+$ (Na$^+$-free) solutions supplemented with 10 μM RR a decrease of extra-mitochondrial Ca$^{2+}$ (fluorescence signal) is representative of [Ca$^{2+}$]m uptake, while an increase in fluorescence signal is indicative of [Ca$^{2+}$]m efflux. Tx, treatment. (E) Quantification of [Ca$^{2+}$]m efflux rates shown in WT: (n = 4 for Na$^+$-free, n = 3 for Na$^+$-containing), in NCLX-KO hepatocytes: (n = 3 for Na$^+$-free, n = 4 for Na$^+$-containing). All values are represented as mean ± SEM, *$p < 0.05$; **$p < 0.01$; ***$p < 0.0001$, N.S- non-significant (two-tailed unpaired *t*-test for comparisons between two groups was used and one-way ANOVA with Tukey's multiple comparison test was used for three or more groups).

mode of Ca$^{2+}$ extrusion and the molecular role of NCLX in liver-isolated mitochondria [32] (Figure 2D). We applied an indirect mitochondrial fluorescent Ca$^{2+}$ monitoring assay that overcomes mitochondrial Ca$^{2+}$ buffering issues using the impermeable acid form of the low-affinity fluorescent Ca$^{2+}$ sensor Oregon Green. We maintained harvested liver mitochondria in an intracellular-mimicking solution with or without Na$^+$ (NMDG$^+$ isosmotically replaced Na$^+$) [26,33,34]. Initially, a Ca$^{2+}$ bolus was added to evoke mitochondrial Ca$^{2+}$ uptake, followed by an addition of a Ca$^{2+}$-free solution without or with Na$^+$ to activate the exchanger, and subsequent increase in the rate of mitochondrial Ca$^{2+}$ removal reflected by the fluorescence rise was monitored (Figure 2E). As in the previous experimental setup, mitochondrial Ca$^{2+}$ efflux demonstrated a strong dependence on the presence of Na$^+$ in the intracellular-mimicking solution and was enhanced by $\sim$ 3-fold compared to Na$^+$-free conditions. In contrast, NCLX KO mitochondria displayed a significant reduction in Ca$^{2+}$ extrusion, with no observed Na$^+$-dependence (Figure 2E). Finally, to further interrogate whether Ca$^{2+}$ efflux is Na$^+$ dependent in human hepatocytes, we utilized HepG2 cells. During Rhod2-AM imaging, Hep2G cells were treated with ATP while maintained in media containing Na$^+$, Li$^+$, or NMDG$^+$. Our results show that Na$^+$ and Li$^+$ activated the mitochondrial Ca$^{2+}$ efflux by $\sim$ 3.5-fold and $\sim$ 2-fold increase, respectively, thereby these results further support an NCLX activity in hepatocytes

(Supplementary Figure 2A—C). Altogether, the results of this part indicate that in hepatocytes, the major Ca$^{2+}$ efflux pathway is predominantly Na$^+$-dependent and mediated by NCLX.

### 3.3. NCLX is indispensable for vasopressin and glucagon-induced oscillations of mitochondrial Ca$^{2+}$

Hepatic hormones, most prominently glucagon and vasopressin (VP), at physiological concentrations, elicit intracellular Ca$^{2+}$ oscillations, which are then propagated individually into the mitochondrial matrix [10,21]. These mitochondrial Ca$^{2+}$ oscillations have a key role in tuning the mitochondrial redox state [7,8,10]. Mechanistically, these oscillatory waves are largely dependent on the IP$_3$R signaling system, yet the mitochondrial players orchestrating these oscillations are not well-characterized [7,9]. Consequently, given the crucial function of NCLX in controlling mitochondrial efflux within the hepatocytes, we sought to study its role in response to glucagon stimuli, which was applied at physiological concentrations to hepatocytes isolated from NCLX cKO mice and their respective controls. Remarkably, while control hepatocytes responded to glucagon with the expected low-frequency intra-cellular and mitochondrial Ca$^{2+}$ oscillations (Figure 3A,C), NCLX cKO hepatocytes exhibited a complete cessation of glucagon-dependent mitochondrial Ca$^{2+}$ oscillations (Figure 3A,B). Intracellular Ca$^{2+}$ oscillations persisted in the NCLX cKO hepatocytes
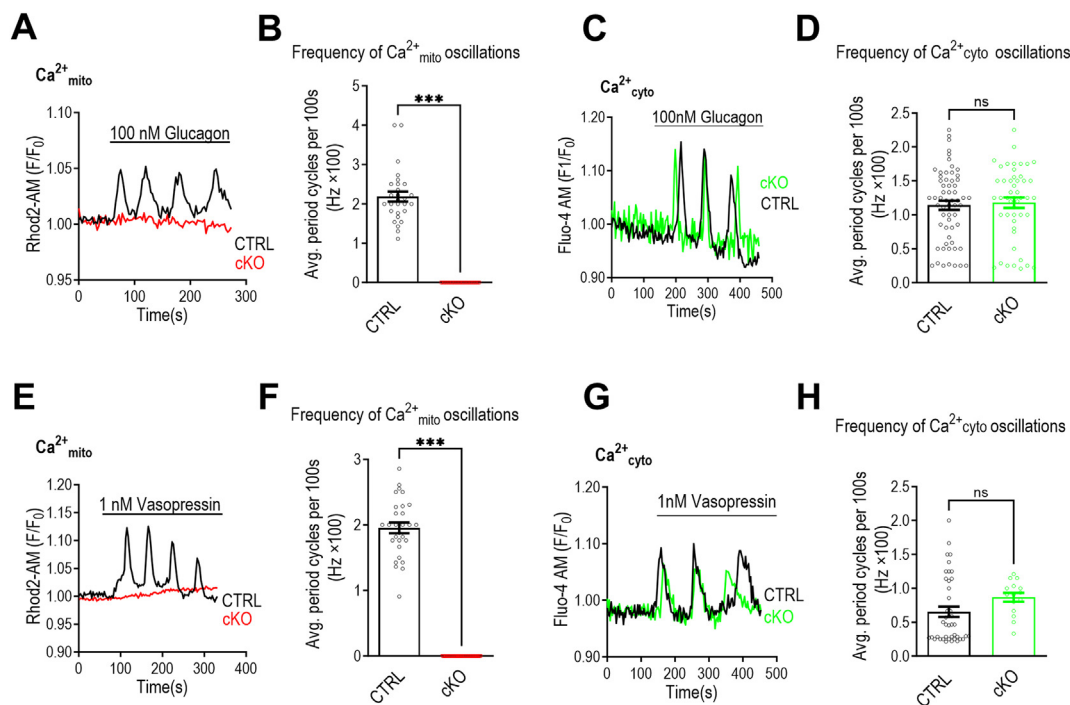
**Figure 3: NCLX is required for Ca$^{2+}$ oscillations generated by physiological concentrations of glucagon and vasopressin.** (A,B) Mitochondrial Ca$^{2+}$ oscillations triggered by physiological concentrations of glucagon in cultured primary hepatocytes isolated from NCLX cKO mice (cKO, Red) and their controls (CTRL, black). [Ca$^{2+}$]m was monitored by Rhod2-AM. (A) Representative fluorescence traces of [Ca$^{2+}$]m, triggered by glucagon (100 nM) in NCLX cKO hepatocytes and their controls (CTRL). (B) Quantification of [Ca$^{2+}$]m frequency of oscillations shown in (A) for CTRL (n = 28) and NCLX cKO hepatocytes (n = 29). (C,D) Cytosolic Ca$^{2+}$ oscillations triggered by physiological concentrations of glucagon in cultured primary hepatocytes isolated from NCLX cKO mice (cKO, Green) and their controls (CTRL, black). Cytosolic Ca$^{2+}$ was monitored by Flou4-AM. (C) Representative fluorescence traces of cytosolic Ca$^{2+}$ oscillations triggered by glucagon (100 nM) in NCLX cKO hepatocytes and their controls (CTRL). (D) Quantification of [Ca$^{2+}$]c frequency of oscillations shown in (C) for CTRL (n = 60) and NCLX cKO hepatocytes (n = 48). (E,F) Mitochondrial Ca$^{2+}$ oscillations triggered by physiological concentrations of vasopressin (VP) in cultured primary hepatocytes isolated from NCLX cKO mice (cKO, Red) and their controls (CTRL, black). Mitochondrial Ca$^{2+}$ was monitored by Rhod2-AM. (E) Representative fluorescence traces of mitochondrial Ca$^{2+}$ oscillations triggered by VP (1 nM) in NCLX cKO hepatocytes and their controls (CTRL). (F) Quantification of mitochondrial Ca$^{2+}$ frequency of oscillations shown in (G) for CTRL (n = 29) and NCLX cKO hepatocytes (n = 42). (G,H) Cytosolic Ca$^{2+}$ oscillations triggered by physiological concentrations of VP in cultured primary hepatocytes isolated from NCLX cKO mice (cKO, Green) and their controls (CTRL, black). Cytosolic Ca$^{2+}$ was monitored by Flou4-AM. (G) Representative fluorescence traces of cytosolic Ca$^{2+}$ oscillations triggered by VP (1 nM) in NCLX cKO hepatocytes and their controls (CTRL). (H) Quantification of [Ca$^{2+}$]c frequency of oscillations shown in (A) for CTRL (n = 42) and NCLX cKO hepatocytes (n = 15). All values are represented as mean ± SEM, *$p < 0.05$; **$p < 0.01$; ****$p < 0.0001$, N.S- non-significant (two-tailed unpaired $t$-test for comparisons between two groups was used).

without an impact on their frequency and showed a modest decrease in area under the curve of the cytosolic Ca$^{2+}$ responses between the NCLX cKO and WT hepatocytes (Figure 3C,D and Supplementary Figure 3A,B). Next, we broadened our analysis to include VP signaling [9,21], which at physiological concentrations as low as 1 nM, triggers intracellular Ca$^{2+}$ oscillations akin to glucagon. Application of VP to WT hepatocytes incited mitochondrial and intracellular Ca$^{2+}$ oscillations, as anticipated (Figure 3E,G). In contrast, VP failed to evoke mitochondrial Ca$^{2+}$ oscillations in NCLX cKO hepatocytes, similar to glucagon, thus further validating the essential role of NCLX in mediating mitochondrial Ca$^{2+}$ oscillations (Figure 3E,F). Again, intracellular Ca$^{2+}$ oscillations and their frequency in the cKO remained largely unaffected compared to the WT, with a modest decrease in the area under the curve of the individual spikes (Figure 3G,H and Supplementary Figure 3C,D). Importantly, the expression of IP$_3$R-1 was not altered in the NCLX cKO livers compared to control, further strengthening the specific effect of NCLX loss on mitochondrial Ca$^{2+}$ oscillations (Supplementary Figure 4A,B).

This set of experiments was then performed in hepatocytes derived from global NCLX KO mice and their WT controls, and consistently demonstrated that while glucagon and VP triggered intracellular and mitochondrial Ca$^{2+}$ oscillations in WT hepatocytes, neither hormone

could induce mitochondrial Ca$^{2+}$ oscillations in the NCLX KO hepatocytes (Supplementary Figure 5A,B, G-H). Intracellular Ca$^{2+}$ oscillations were largely preserved across both genotypes and no disparity in the magnitude of cytosolic Ca$^{2+}$ responses were noted, albeit with a modest decrease of cytosolic Ca$^{2+}$ oscillation frequency only with VP in the global NCLX KO hepatocytes (Supplementary Figure 5A-L).

In summary, these findings show that NCLX is a key regulator for mitochondrial Ca$^{2+}$ oscillations evoked by hepatic hormones, underscoring the physiological role of NCLX in hepatic mitochondrial calcium signaling.
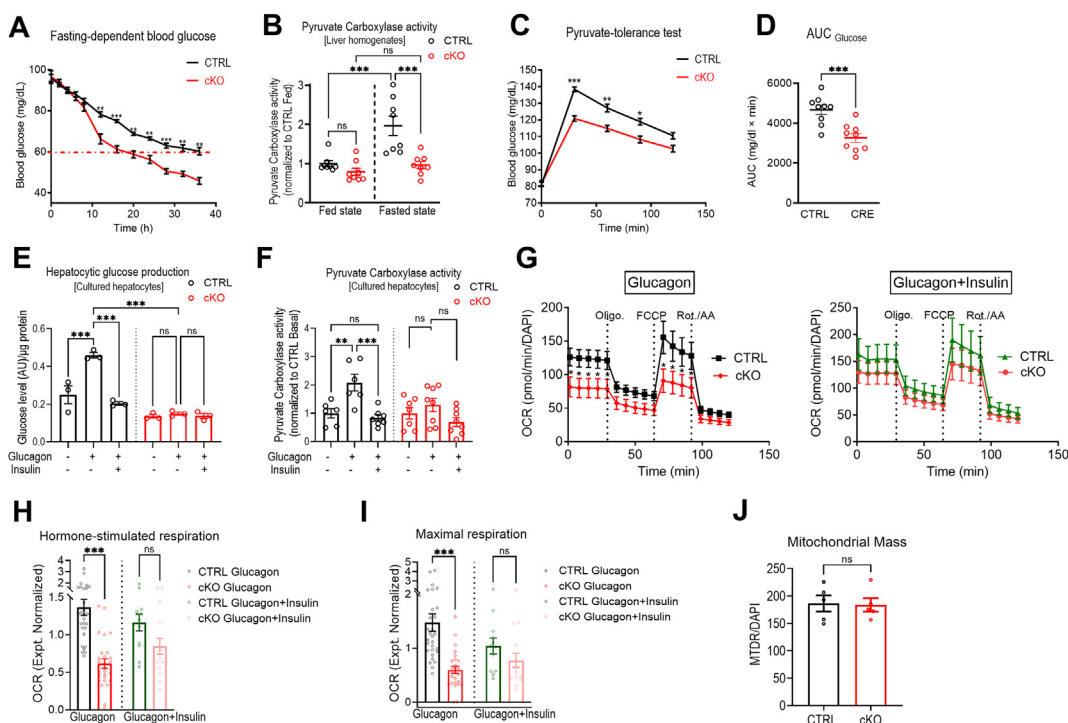
### 3.4. NCLX is essential for glucagon-mediated hepatic gluconeogenesis

Considering the significant role of NCLX in facilitating glucagon-dependent mitochondrial Ca$^{2+}$ oscillations, we hypothesized that NCLX activity is essential for glucagon-dependent gluconeogenesis. To investigate the potential role of NCLX in hepatic glucose production (HGP), we first continuously monitored blood glucose levels in hepatic NCLX cKO mice and their control littermates under fasting conditions (Figure 4A). Interestingly, while no discernible difference was observed during the initial 8 h (which corresponds to the time required to deplete glycogen stores), a subsequent steady-fast decline in blood glucose

levels was noted in the NCLX cKO mice. This decline continued until their blood glucose levels reached hypoglycemic levels, defined by a 60 mg/dL cut-off, in contrast to the control mice, which maintained significantly higher blood glucose concentrations (Figure 4A).

Under fasting conditions, an elevated glucagon/insulin ratio shunts circulating lactate and pyruvate from oxidation towards anaplerosis. Hepatic pyruvate carboxylase (PC) is the principal anaplerotic pathway and a rate-controlling factor for gluconeogenesis [11,13,35]. To confirm that HGP primarily arises from compromised glucagon-stimulated gluconeogenesis in the NCLX cKO livers, we utilized different complementary in vivo and in vitro approaches. First, assessment of liver homogenates isolated from fasted and fed NCLX cKO and their controls revealed a significant increase in PC activity rate in the fasted control mice, while NCLX cKO mice failed to increase PC activity upon fasting (Figure 4B). Next, to gauge hepatic gluconeogenesis in NCLX cKO mice and their controls, we utilized the pyruvate tolerance test and quantified the conversion rate of the perfused substrate into glucose. Notably, while injection of pyruvate in fasted mice produced a significant glucose excursion in the controls, NCLX

cKO glucose production rate was significantly lower by over 30% as indicated by the calculated area under the curve, thus further suggesting a compromised gluconeogenesis process, which is independent of the substrate availability for PC (Figure 4C,D).

Prolonged fasting can lead to a shift in hormonal balance, potentially affecting the gluconeogenic function of hepatocytes through altered hormonal balance [36]. To determine the role of glucagon on hepatic glucose production (HGP), we evaluated glucagon-induced glucose production in cultured hepatocytes isolated from NCLX cKO mice and their control littermates (Figure 4E). Consistent with the in vivo study done in fasted mice, glucagon enhanced glucose production in cultured hepatocytes isolated from control mice. The addition of insulin to glucagon, however, blunted the rise. In contrast to the control hepatocytes, glucagon failed to stimulate glucose production in NCLX cKO hepatocytes and resulted in glucose levels similar to those produced from unstimulated hepatocytes or those co-stimulated with insulin and glucagon. We then measured PC activity in cultured primary hepatocytes. As anticipated, glucagon stimulation led to an increase in the enzyme activity rate compared to baseline or to concurrent insulin



**Figure 4: NCLX is required for glucagon-mediated hepatic glucose production.** (A) Blood glucose measurements at indicated time intervals in mice during fasting from NCLX cKO (cKO) and CTRL mice (n = 4 each). The dashed red line indicates the lower threshold of physiological glycemic control (60 mg/dL). (B) Hepatic pyruvate carboxylase activity determined in liver homogenates from - NCLX cKO and CTRL in fed and fasted conditions (n = 8 for each condition). (C) pyruvate tolerant test (PTT) plot for NCLX cKO and CTRL mice fasted for 8 h (n = 9 for each condition). (D) Area under the curve (AUC) for the glycemic responses in (C). (E) Gluconeogenesis assessed by glucose production in response to lactate and pyruvate in cultured primary mouse hepatocytes isolated from NCLX cKO and CTRL mice. Glucagon (100 nM) was used to induce gluconeogenesis. Co-administration of insulin (100 nM) with glucagon was used as a negative control (n = 3 for each condition). (F) Hepatic pyruvate carboxylase activity assessed in response to lactate and pyruvate in cultured primary mouse hepatocytes from NCLX cKO and CTRL mice (For basal enzymatic activity n = 6 CTRL and n = 7 cKO; For glucagon stimulation n = 6 CTRL and n = 8 cKO; for co-stimulation of insulin and glucagon n = 7 CTRL and n = 8 cKO). (G−I) Oxygen consumption rates (OCR) of NCLX cKO and CTRL primary hepatocytes pre-treated either with glucagon alone *(left panel)* or co-treated with insulin and glucagon *(right panel)*. (G) Representative OCR traces of NCLX cKO and CTRL primary hepatocytes pre-treated with glucagon *(left panel)* or co-treated with insulin and glucagon *(right panel)*. Oxygen consumption was measured in real-time under basal conditions and in response to indicated mitochondrial modulating compounds. (H) Quantification of hormonal stimulatory response in primary hepatocytes, for glucagon stimulation n = 29 CTRL and n = 27 NCLX cKO; for insulin and glucagon co-stimulation n = 12 CTRL and n = 15 NCLX cKO. OCR values were normalized to the average OCR of all traces. (I) Quantification of maximal respiration induced by FCCP in primary hepatocytes, for glucagon stimulation n = 29 CTRL and n = 27 NCLX cKO; for insulin and glucagon co-stimulation n = 12 CTRL and n = 15 NCLX cKO (CRE). OCR values were normalized to the average OCR of all traces. (J) Mitochondrial mass assessed by MTDR staining in plated primary hepatocytes (n = 5 for each genotype). All values are represented as mean ± SEM, $*p < 0.05$; $**p < 0.01$; $****p < 0.0001$, N.S- non-significant (two-tailed unpaired $t$-test for comparisons between two groups was used and one-way ANOVA with Tukey's multiple comparison test was used for three or more groups).

and glucagon co-stimulation, in which insulin blunted glucagon's effect (Figure 4F). However, in NCLX cKO hepatocytes, no significant differences were observed in PC activity following stimulation with glucagon alone in comparison to the baseline and co-stimulation with insulin and glucagon (Figure 4F). Notably, the observed reduction rates of HGP occurred in the absence of any alteration to transcriptionally regulated key hepatic gluconeogenic genes such as PEPCK and G6Pase, quantified from NCLX cKO livers and their controls under fasting conditions (Supplementary Figure 6A). This further suggests an acute, transcriptionally-independent role for NCLX in the regulation of gluconeogenesis.

Altogether, these in vivo and in vitro results demonstrate that NCLX plays a critical role in hepatic glucose production by controlling the glucagon-dependent mitochondrial $Ca^{2+}$ signaling.

To elucidate the metabolic role of NCLX in mediating glucagon-induced mitochondrial $Ca^{2+}$ oscillations and hepatic gluconeogenic function, we conducted a seahorse respirometry analysis. This experimental approach was applied to isolated hepatocytes originating from conditional NCLX KO and their control littermates (Figure 4G). Upon subjecting the hepatocytes to glucagon pre-treatment, we observed substantial impairments in hormone-stimulated OCR and maximal respiratory capacities in the conditional NCLX KO hepatocytes (Figure 4H,I). Staining both genotypes with a mitochondrial dye (MTDR) did not reveal a discernible change in mitochondrial mass (Figure 4J), and OCR monitoring under unstimulated conditions did not show significant metabolic alterations (Supplementary Figure 7A,B). Thus, the bioenergetic findings are indicative of an impact on mitochondrial function and suggest a potential association between NCLX and the regulation of hepatic metabolism in response to glucagon stimulation. Conversely, pre-treatment of insulin and glucagon did not reveal any significant differences when comparing the two genotypes (Figure 4G–I), indicating that the metabolic status of NCLX KO hepatocytes remains largely intact. However, their glucagon-dependent gluconeogenesis and related pathways are selectively impaired. The absence of observable alterations in insulin response between the genotypes underscores the specificity and selectivity of NCLX in regulating hepatic metabolic and hormonal homeostasis.

Altogether, this set of in vivo and in vitro results indicate that NCLX plays a critical role in mediating hepatic glucose production by controlling glucagon-dependent mitochondrial $Ca^{2+}$ signaling.

## 4. DISCUSSION

The molecular identity accountable for mitochondrial $Ca^{2+}$ extrusion in the hepatocyte has been debated for a long time, and multiple mechanisms have been suggested. Our study demonstrates for the first time that NCLX is indispensable for mitochondrial calcium extrusion in hepatocytes. Furthermore, our results indicate that a $Na^+$-dependent activity is the major route for mitochondrial $Ca^{2+}$ efflux and that the presence of extracellular $Na^+$ is required to fully activate $Ca^{2+}$ extrusion. We used intact or permeabilized cells, isolated mitochondria, and investigated the exchanger in a human hepatocyte cell-line as well as two mice models, a global NCLX KO and a conditional hepatic NCLX KO system. Notably, the presence of $Na^+$ in cells and mitochondrial preparations enhanced mitochondrial $Ca^{2+}$ efflux by $\sim$ 3-fold. In contrast, the presence or absence of extracellular $Na^+$ in KO-derived hepatocytes failed to enhance the $Ca^{2+}$ efflux pathway in either system. Moreover, $Na^+$ influx via the cell membrane is required for full activation of the mitochondrial $Na^+/Ca^{2+}$ exchanger, consistent with reports demonstrating a low affinity of NCLX for cytosolic $Na^+$ [4,28].

What is the basis for the differences in the present and previous studies that supported a $Na^+$-independent primary mechanism for mitochondrial $Ca^{2+}$ efflux in hepatocytes [14]? First, many of these studies were conducted on isolated mitochondria that often lose their mitochondrial membrane potential following their isolation. Notably, even a small drop of mitochondrial $\Delta\Psi$ is sufficient to inhibit $Na^+$-dependent mitochondrial $Ca^{2+}$ efflux by NCLX [34,37]. Interestingly, isolated liver mitochondria from energized hepatocytes, treated with a beta-adrenergic receptor agonist, restored the $Na^+$-dependent $Ca^{2+}$ efflux system [32]. Thus, if the isolated mitochondria were not fully energized, mitochondrial $Na^+$-dependent $Ca^{2+}$ efflux could have been impaired. A $Na^+$-independent mitochondrial $Ca^{2+}$ efflux was also suggested in a study conducted on cultured hepatocytes, which compared their mitochondrial $Ca^{2+}$ efflux to cardiomyocytes and neuronal cells [15]. The reasons for the differences between this and our study are unclear. However, the former study was done on primary hepatocytes 7 days post their culturing, a timeline which may lead to hepatocyte de-differentiation [38]. Moreover, mitochondrial $Ca^{2+}$ efflux in this study was exceedingly 100-fold slower than rates found in previous reports and our studies, indicating that the mitochondrial $Ca^{2+}$ efflux was largely inactive [15].

Hepatic stimulation by glucagon and other hepatic hormones at low physiological concentrations, that are sufficient to facilitate $Ca^{2+}$ release from the ER stores into the cytoplasm, evoke low-frequency cytosolic $Ca^{2+}$ oscillation spikes. Importantly, these spikes are transmitted individually into the mitochondrial matrix, enhancing the metabolic activity [9,10,21]. Our results show that while deletion of hepatic NCLX has a subtle effect on glucagon and VP induced cytosolic oscillations, it triggers a profound inhibition of glucagon-dependent mitochondrial $Ca^{2+}$ oscillations. What is the molecular basis for this effect of NCLX on mitochondrial $Ca^{2+}$ oscillations? Previous studies indicated that mitochondrial $Ca^{2+}$ influx by MCU is downregulated by even a subtle rise in mitochondrial free $Ca^{2+}$, a process that is tuned by EMRE and Micu1 [23,39–42]. Consistent with these findings, mitochondrial $Ca^{2+}$ oscillations are triggered by caffeine in neurons and are suppressed by NCLX KO, which causes mitochondrial $Ca^{2+}$ overload [43]. It should be noted that mitochondrial $Ca^{2+}$ influx was intact when we used pharmacological concentration of ATP to evoke a monophasic $Ca^{2+}$ purinergic response. Further studies are required to determine what is the effect of hepatic NCLX KO on the composition and regulation of the MCU complex in the presence of physiological concentrations of hepatic hormones that evoke the oscillatory cytosolic and mitochondrial $Ca^{2+}$ responses under physiological and pharmacological concentrations.

The role of $Ca^{2+}$ signaling in controlling metabolic activity and gluconeogenesis is of intense interest [13]. Furthermore, a recent study on caloric restriction models indicated that NCLX plays a pivotal role in regulating basal and starvation-induced autophagy in the liver [44], further linking NCLX's role in regulating hepatic metabolic response to overall nutritional state. Studies using the hepatic hormones or other agonists, often evoked a strong single cytosolic and mitochondrial $Ca^{2+}$ response when employed at pharmacological concentration and not the hallmark oscillatory response encountered during physiological activity [12,13]. Our studies, conducted at physiological concentrations, show that impairing the $Ca^{2+}$ oscillatory pattern activated by glucagon and VP in the KO model of NCLX is sufficient to affect both the metabolic activity and gluconeogenesis. Another unresolved matter, is the distinct role of the hormone-dependent cytosolic or mitochondrial $Ca^{2+}$ response in hepatic gluconeogenesis [21]. While a mitochondrial $Ca^{2+}$ rise is linked to metabolic regulation, many other studies underscore the importance of

extra-mitochondrial pathways in mediating the $Ca^{2+}$-dependent metabolic changes, most notably the Aralar pathway in neurons and cardiomyocytes [45]. The hepatic KO of NCLX offers a unique paradigm to address this issue because, in using this model, the hormone-dependent cytosolic $Ca^{2+}$ oscillations are fully preserved while the mitochondria are suppressed. Our results further indicate that the suppression of the mitochondrial $Ca^{2+}$ oscillations is associated with the reduction of the glucagon-dependent mitochondrial metabolic activity and gluconeogenesis, thus underscoring the dominant role of mitochondrial $Ca^{2+}$ signaling in this process. While this study elucidates the crucial role of glucagon-mediated $Ca^{2+}$ oscillation in regulating gluconeogenesis and metabolism, the specific downstream metabolic processes influenced by these oscillations remain unclear. Notably, although our study and previous research have established a connection between $Ca^{2+}$ signaling and regulating overall mitochondrial metabolism and redox state [8,21,36,46], it is yet to determine what is the distinctive role of $Ca^{2+}$ oscillations in regulating mitochondrial respirometry. Despite being highly valuable and reliable, the seahorse respirometry analysis lacks the necessary single-cell resolution and temporal resolution. Therefore, understanding the mechanism of glucagon's mode of action in stimulating hepatic respiration will necessitate the use of faster single-cell analysis techniques that are currently unavailable. Our study also raises several other fundamental questions that will be addressed in future studies. Among them what is the role of NCLX in tuning the glucagon receptor and the downstream PKA signaling and CREB activation? Or what is the role of NCLX-dependent $Ca^{2+}$ signaling in hepatic lipid metabolism?

## 5. CONCLUSIONS

The results of this study reveal that NCLX plays an essential role in regulating hepatic mitochondrial calcium extrusion in a $Na^+$-dependent manner. It underscores the physiological role of NCLX in controlling mitochondrial $Ca^{2+}$ oscillations required for efficient electron transport chain and oxidative phosphorylation. Lastly, this study sheds light on the metabolic role of NCLX in glucagon-mediated $Ca^{2+}$ signaling, which by facilitating the transmission of cytosolic $Ca^{2+}$ oscillations to mitochondria, drives the hepatic transcription-independent gluconeogenesis pathway.

## CREDIT AUTHORSHIP CONTRIBUTION STATEMENT

**Mahmoud Taha:** Writing — review & editing, Writing — original draft, Methodology, Investigation, Formal analysis, Data curation. **Essam A. Assali:** Writing — review & editing, Writing — original draft, Methodology, Investigation, Formal analysis, Data curation, Supervision, Conceptualization. **Tsipi Ben-Kasus Nissim:** Formal analysis, Data curation. **Grace E. Stutzmann:** Writing — review & editing, Funding acquisition, Conceptualization. **Orian S. Shirihai:** Writing — review & editing, Conceptualization. **Michal Hershfinkel:** Writing — review & editing, Methodology. **Israel Sekler:** Writing — review & editing, Writing — original draft, Supervision, Funding acquisition, Data curation, Conceptualization.

## ACKNOWLEDGEMENTS

## DECLARATION OF COMPETING INTEREST

The authors declare no conflict of interest.

## DATA AVAILABILITY

Data will be made available on request.

## APPENDIX A. SUPPLEMENTARY DATA

Supplementary data to this article can be found online at https://doi.org/10.1016/j.molmet.2024.101982.

## REFERENCES

[1] Szabadkai G, Duchen MR. Mitochondria: the hub of cellular Ca2+ signaling. Physiology 2008;23:84—94. https://doi.org/10.1152/physiol.00046.2007.

[2] Giorgi C, Marchi S, Pinton P. The machineries, regulation and cellular functions of mitochondrial calcium. Nat Rev Mol Cell Biol 2018;19(11):713—30. https://doi.org/10.1038/s41580-018-0052-8.

[3] Kamer KJ, Mootha VK. The molecular era of the mitochondrial calcium uniporter. Nat Rev Mol Cell Biol 2015;16(9):545—53. https://doi.org/10.1038/nrm4039.

[4] Palty R, Silverman WF, Hershfinkel M, Caporale T, Sensi SL, Parnis J, et al. NCLX is an essential component of mitochondrial Na+/Ca2+ exchange. Proc Natl Acad Sci USA 2010;107(1):436—41. https://doi.org/10.1073/pnas.0908099107.

[5] Loncke J, Kaasik A, Bezprozvanny I, Parys JB, Kerkhofs M, Bultynck G. Balancing ER-mitochondrial Ca(2+) fluxes in health and disease. Trends Cell Biol 2021;31(7):598—612. https://doi.org/10.1016/j.tcb.2021.02.003.

[6] Katona M, Bartók Á, Nichtova Z, Csordás G, Berezhnaya E, Weaver D, et al. Capture at the ER-mitochondrial contacts licenses IP(3) receptors to stimulate local Ca(2+) transfer and oxidative metabolism. Nat Commun 2022;13(1): 6779. https://doi.org/10.1038/s41467-022-34365-8.

[7] Hajnóczky G, Robb-Gaspers LD, Seitz MB, Thomas AP. Decoding of cytosolic calcium oscillations in the mitochondria. Cell 1995;82(3):415—24. https://doi.org/10.1016/0092-8674(95)90430-1.

[8] Griffiths EJ, Rutter GA. Mitochondrial calcium as a key regulator of mitochondrial ATP production in mammalian cells. Biochim Biophys Acta 2009;1787(11):1324—33. https://doi.org/10.1016/j.bbabio.2009.01.019.

[9] Paillard M, Csordás G, Szanda G, Golenár T, Debattisti V, Bartok A, et al. Tissue-specific mitochondrial decoding of cytoplasmic Ca(2+) signals is controlled by the stoichiometry of MICU1/2 and MCU. Cell Rep 2017;18(10): 2291—300. https://doi.org/10.1016/j.celrep.2017.02.032.

[10] Robb-Gaspers LD, Burnett P, Rutter GA, Denton RM, Rizzuto R, Thomas AP. Integrating cytosolic calcium signals into mitochondrial metabolic responses. EMBO J 1998;17(17):4987—5000. https://doi.org/10.1093/emboj/17.17.4987.

[11] Han H-S, Kang G, Kim JS, Choi BH, Koo S-H. Regulation of glucose metabolism from a liver-centric perspective. Exp Mol Med 2016;48(3):e218. https://doi.org/10.1038/emm.2015.122.

[12] Wang Y, Li G, Goode J, Paz JC, Ouyang K, Screaton R, et al. Inositol-1,4,5-trisphosphate receptor regulates hepatic gluconeogenesis in fasting and diabetes. Nature 2012;485(7396):128—32. https://doi.org/10.1038/nature10988.

[13] Perry RJ, Zhang D, Guerra MT, Brill AL, Goedeke L, Nasiri AR, et al. Glucagon stimulates gluconeogenesis by INSP3R1-mediated hepatic lipolysis. Nature 2020;579(7798):279—83. https://doi.org/10.1038/s41586-020-2074-6.

[14] Fiskum G, Lehninger AL. Regulated release of Ca2+ from respiring mitochondria by Ca2+/2H+ antiport. J Biol Chem 1979;254(14):6236—9.

[15] Rysted JE, Lin Z, Walters GC, Rauckhorst AJ, Noterman M, Liu G, et al. Distinct properties of Ca(2+) efflux from brain, heart and liver mitochondria: the effects of Na(+), Li(+) and the mitochondrial Na(+)/Ca(2+) exchange inhibitor CGP37157. Cell Calcium 2021;96:102382. https://doi.org/10.1016/j.ceca.2021.102382.

[16] Crompton M, Kunzi M, Carafoli E. The calcium-induced and sodium-induced effluxes of calcium from heart mitochondria. Evidence for a sodium-calcium carrier. Eur J Biochem 1977;79(2):549—58. https://doi.org/10.1111/j.1432-1033.1977.tb11839.x.

[17] Crompton M, Heid I. The cycling of calcium, sodium, and protons across the inner membrane of cardiac mitochondria. Eur J Biochem 1978;91(2):599—608. https://doi.org/10.1111/j.1432-1033.1978.tb12713.x.

[18] Wingrove DE, Gunter TE. Kinetics of mitochondrial calcium transport. I. Characteristics of the sodium-independent calcium efflux mechanism of liver mitochondria. J Biol Chem 1986;261(32):15159—65.

[19] Drago I, Pizzo P, Pozzan T. After half a century mitochondrial calcium in- and efflux machineries reveal themselves. EMBO J 2011;30(20):4119—25. https://doi.org/10.1038/emboj.2011.337.

[20] Luongo TS, Lambert JP, Gross P, Nwokedi M, Lombardi AA, Shanmughapriya S, et al. The mitochondrial Na(+)/Ca(2+) exchanger is essential for Ca(2+) homeostasis and viability. Nature 2017;545(7652):93—7. https://doi.org/10.1038/nature22082.

[21] Hajnoczky G, Robb-Gaspers LD, Seitz MB, Thomas AP. Decoding of cytosolic calcium oscillations in the mitochondria. Cell 1995;82(3):415—24.

[22] Rooney TA, Sass EJ, Thomas AP. Characterization of cytosolic calcium oscillations induced by phenylephrine and vasopressin in single fura-2-loaded hepatocytes. J Biol Chem 1989;264(29):17131—41.

[23] Antony AN, Paillard M, Moffat C, Juskeviciute E, Correnti J, Bolon B, et al. MICU1 regulation of mitochondrial Ca(2+) uptake dictates survival and tissue regeneration. Nat Commun 2016;7:10955. https://doi.org/10.1038/ncomms10955.

[24] Goldstone TP, Duddridge RJ, Crompton M. The activation of Na+-dependent efflux of Ca2+ from liver mitochondria by glucagon and beta-adrenergic agonists. Biochem J 1983;210(2):463—72. https://doi.org/10.1042/bj2100463.

[25] Renault TT, Luna-Vargas MPA, Chipuk JE. Mouse liver mitochondria isolation, size fractionation, and real-time MOMP measurement. Bio-Protocol 2016;6(15). https://doi.org/10.21769/BioProtoc.1892.

[26] Kowaltowski AJ, Menezes-Filho SL, Assali EA, Gonçalves IG, Cabral-Costa JV, Abreu P, et al. Mitochondrial morphology regulates organellar Ca(2+) uptake and changes cellular Ca(2+) homeostasis. FASEB (Fed Am Soc Exp Biol) J : Off Pub Feder Am Soci Exp Biol 2019;33(12):13176—88. https://doi.org/10.1096/fj.201901136R.

[27] Kostic M, Ludtmann MHR, Bading H, Hershfinkel M, Steer E, Chu CT, et al. PKA phosphorylation of NCLX reverses mitochondrial calcium overload and depolarization, promoting survival of PINK1-deficient dopaminergic neurons. Cell Rep 2015;13(2):376—86. https://doi.org/10.1016/j.celrep.2015.08.079.

[28] Palty R, Ohana E, Hershfinkel M, Volokita M, Elgazar V, Beharier O, et al. Lithium-calcium exchange is mediated by a distinct potassium-independent sodium-calcium exchanger. J Biol Chem 2004;279(24):25234—40. https://doi.org/10.1074/jbc.M401229200.

[29] Assali EA, Jones AE, Veliova M, Acín-Pérez R, Taha M, Miller N, et al. NCLX prevents cell death during adrenergic activation of the brown adipose tissue. Nat Commun 2020;11(1):3347. https://doi.org/10.1038/s41467-020-16572-3.

[30] Ngo J, Choi DW, Stanley IA, Stiles L, Molina AJA, Chen P-H, et al. Mitochondrial morphology controls fatty acid utilization by changing CPT1 sensitivity to malonyl-CoA. EMBO J 2023;42(11):e111901. https://doi.org/10.15252/embj.2022111901.

[31] Jadiya P, Cohen HM, Kolmetzky DW, Kadam AA, Tomar D, Elrod JW. Neuronal loss of NCLX-dependent mitochondrial calcium efflux mediates age-associated cognitive decline. iScience 2023;26(3):106296. https://doi.org/10.1016/j.isci.2023.106296.

[32] Goldstone TP, Crompton M. Evidence for beta-adrenergic activation of Na+-dependent efflux of Ca2+ from isolated liver mitochondria. Biochem J 1982;204(1):369—71. https://doi.org/10.1042/bj2040369.

[33] Boyman L, Karbowski M, Lederer WJ. Regulation of mitochondrial ATP production: Ca(2+) signaling and quality control. Trends Mol Med 2020;26(1):21—39. https://doi.org/10.1016/j.molmed.2019.10.007.

[34] Boyman L, Coleman AK, Zhao G, Wescott AP, Joca HC, Greiser BM, et al. Dynamics of the mitochondrial permeability transition pore: transient and permanent opening events. Arch Biochem Biophys 2019;666:31—9. https://doi.org/10.1016/j.abb.2019.03.016.

[35] Cappel DA, Deja S, Duarte JAG, Kucejova B, Iñigo M, Fletcher JA, et al. Pyruvate-carboxylase-mediated anaplerosis promotes antioxidant capacity by sustaining TCA cycle and redox metabolism in liver. Cell Metabol 2019;29(6):1291—1305.e8. https://doi.org/10.1016/j.cmet.2019.03.014.

[36] Petersen MC, Vatner DF, Shulman GI. Regulation of hepatic glucose metabolism in health and disease. Nat Rev Endocrinol 2017;13(10):572—87. https://doi.org/10.1038/nrendo.2017.80.

[37] Kostic M, Katoshevski T, Sekler I. Allosteric regulation of NCLX by mitochondrial membrane potential links the metabolic state and Ca(2+) signaling in mitochondria. Cell Rep 2018;25(12):3465—3475.e4. https://doi.org/10.1016/j.celrep.2018.11.084.

[38] Hu C, Li L. In vitro culture of isolated primary hepatocytes and stem cell-derived hepatocyte-like cells for liver regeneration. Protein & Cell 2015;6(8):562—74. https://doi.org/10.1007/s13238-015-0180-2.

[39] Samanta K, Douglas S, Parekh AB. Mitochondrial calcium uniporter MCU supports cytoplasmic Ca2+ oscillations, store-operated Ca2+ entry and Ca2+-dependent gene expression in response to receptor stimulation. PLoS One 2014;9(7):e101188. https://doi.org/10.1371/journal.pone.0101188.

[40] Vais H, Mallilankaraman K, Mak D-OD, Hoff H, Payne R, Tanis JE, et al. EMRE is a matrix Ca(2+) sensor that governs gatekeeping of the mitochondrial Ca(2+) uniporter. Cell Rep 2016;14(3):403—10. https://doi.org/10.1016/j.celrep.2015.12.054.

[41] Csordás G, Golenár T, Seifert EL, Kamer KJ, Sancak Y, Perocchi F, et al. MICU1 controls both the threshold and cooperative activation of the mitochondrial Ca2+ uniporter. Cell Metabol 2013;17(6):976—87. https://doi.org/10.1016/j.cmet.2013.04.020.

[42] Moreau B, Nelson C, Parekh AB. Biphasic regulation of mitochondrial Ca2+ uptake by cytosolic Ca2+ concentration. Curr Biol : CB 2006;16(16):1672—7. https://doi.org/10.1016/j.cub.2006.06.059.

[43] Rozenfeld M, Azoulay IS, Ben Kasus Nissim T, Stavsky A, Melamed M, Stutzmann G, et al. Essential role of the mitochondrial Na(+)/Ca(2+) exchanger NCLX in mediating PDE2-dependent neuronal survival and learning. Cell Rep 2022;41(10):111772. https://doi.org/10.1016/j.celrep.2022.111772.

[44] Ramos VM, Serna JDC, Vilas-Boas EA, Cabral-Costa JV, Cunha FM, Kataura T, et al. Mitochondrial sodium/calcium exchanger (NCLX) regulates basal and starvation-induced autophagy through calcium signaling. FASEB (Fed Am Soc Exp Biol) J : Off Pub Feder Am Soci Exp Biol 2024;38(3):e23454. https://doi.org/10.1096/fj.202301368RR.

[45] Pérez-Liébana I, Juaristi I, González-Sánchez P, González-Moreno L, Rial E, Podunavac M, et al. A Ca(2+)-dependent mechanism boosting glycolysis and OXPHOS by activating aralar-malate-aspartate shuttle, upon neuronal stimulation. J Neurosci : Off J Soci Neurosci 2022;42(19):3879—95. https://doi.org/10.1523/JNEUROSCI.1463-21.2022.

[46] Amigo I, Traba J, González-Barroso MM, Rueda CB, Fernández M, Rial E, et al. Glucagon regulation of oxidative phosphorylation requires an increase in matrix adenine nucleotide content through Ca2+ activation of the mitochondrial ATP-Mg/Pi carrier SCaMC-3. J Biol Chem 2013;288(11):7791—802. https://doi.org/10.1074/jbc.M112.409144.